

A windowless design for the target of the EADF

S. Buono, L. Maciocco, V. Moreau, L. Sorrentino

CRS4, Centre for Advanced Studies, Research and Development in Sardinia

May 10th 2001

Abstract

In this note, we review the main features of the windowless target requirement. Then, we derive some necessary characteristics of the flow. We also make some comments hopefully useful for an eventual design optimisation process. From a first analysis, it seems that the requirements imposed on the maximum temperature and the pressure losses can be met but care must be taken to avoid a buoyancy induced flow critical instability.

Contents

1	Introduction.....	2
2	Geometrical Description	2
3	Physical Constraints.....	2
3.1	Global constraints.....	2
3.2	Physical properties.....	3
3.3	Beam properties.....	3
3.4	Flow properties.....	6
4	Flow tailoring.....	7
4.1	Flow horizontality	7
4.2	Horizontal flow tailoring	10
4.3	Vertical flow tailoring	12
4.4	Channel separation	12
5	Optimisation past history	13
5.1	Single channel optimisation trial	13
5.2	Optimisation of the channel splitting	21
5.3	Encountered problems	23
6	Buoyancy pressure drop.....	28
7	Beam radius optimisation	28
8	Conclusions.....	29
9	References.....	30

1 Introduction

In the framework of the Energy Amplifier Demonstration Facility, two options are contemplated for the spallation target: a target with a solid window and a windowless target. Advantages and drawbacks of these options are analysed elsewhere. In this note, we will give the system requirements and derive some considerations on the necessary flow structure. It has been raised necessary to understand the in-out of the induced geometrical constraint and flow features.

2 Geometrical Description

The geometrical constraints are quite few (Table 1). The windowless target must be inserted in a vertical cylinder of diameter 52 cm. The proton beam penetration is about 28 cm, so we consider that the target height must be at least 30 cm. The inlet flow comes from below and the outlet flows downward.

Parameter (symbol)	Value
Diameter (D)	≤ 52 cm
Height (H)	≥ 30 cm

Table 1: main geometrical parameters.

3 Physical Constraints

3.1 Global constraints

The mass flow rate is:

$$m = 150 \text{ kg/s}$$

The pressure loss ΔP (out of the buoyancy pressure drop) must be confined below $\Delta P_{\max} = 5000$ Pa. The proton beam intensity is 6 mA for a total power release of $P_{\text{ow}} = 2.545$ MW. The beam radius (parabolic profile) is free and will be considered, unless otherwise specified, to be $R = 6$ cm in all the following. The temperature in inlet is always considered to be $T_0 = 300$ C. The maximum increase of temperature between the inlet and the surface level must be kept under $\Delta T_{\max} = 150$ K. The maximum bulk temperature must not reach the boiling point. The maximum wall temperature is not clearly defined but must be kept as low as possible, with a special attention to avoid strong gradients. Most of these constraints are resumed in Table 2.

Parameter (symbol)	Value
Mass flow rate (m)	150 kg/s
Inlet temperature (T_0)	300 C
Maximum pressure loss (ΔP_{\max})	5000 Pa
Total power release (P_{ow})	2.545 MW

Beam radius (R)	6 cm
Maximum surface temperature increase (ΔT_{\max})	150 K

Table 2: Main physical constraints

3.2 Physical properties

The fluid used is the lead-bismuth eutectic, whose main physical properties are reported in Table 3.

Parameter (symbol) [units]	Formula (temperature in K)	Value at 300 C	Value at 400 C	Value at 500 C
Density (ρ_w) [kg/m ³]	$11112. - 1.37 T$	10327	10190	10053
Molecular viscosity(μ) [m ² /s]	$4.71 \cdot 10^{-9} T^2 - 8.92 \cdot 10^{-6} T + 5.37 \cdot 10^{-3}$	$1.81 \cdot 10^{-3}$	$1.5 \cdot 10^{-3}$	$1.29 \cdot 10^{-3}$
Surface tension(σ) [N/m]	$0.473 - 1.03 \cdot 10^{-4} T$	0.414	0.404	0.395
Thermal conductivity(k) [W/kg/K]	$3.03 \cdot 10^{-5} T^2 - 1.83 \cdot 10^{-2} T + 11.48$	11.0	12.9	15.4
Specific heat(C_p) [J/kg/K]	146.5	146.5	146.5	146.5

Table 3: Physical properties of the Pb-Bi eutectic

3.3 Beam properties

The proton beam is vertical (going downward) and has a parabolic energy distribution profile. The radius of the parabolic profile can be optimised but is considered to be $R = 6$ cm in this section. The beam is expected to invest the molten lead through a somewhat flat liquid surface. The beam penetration is about 28 cm, with a heat deposition decreasing slowly and showing a small peak (Brag peak) before vanishing., as shown in Figure 1.

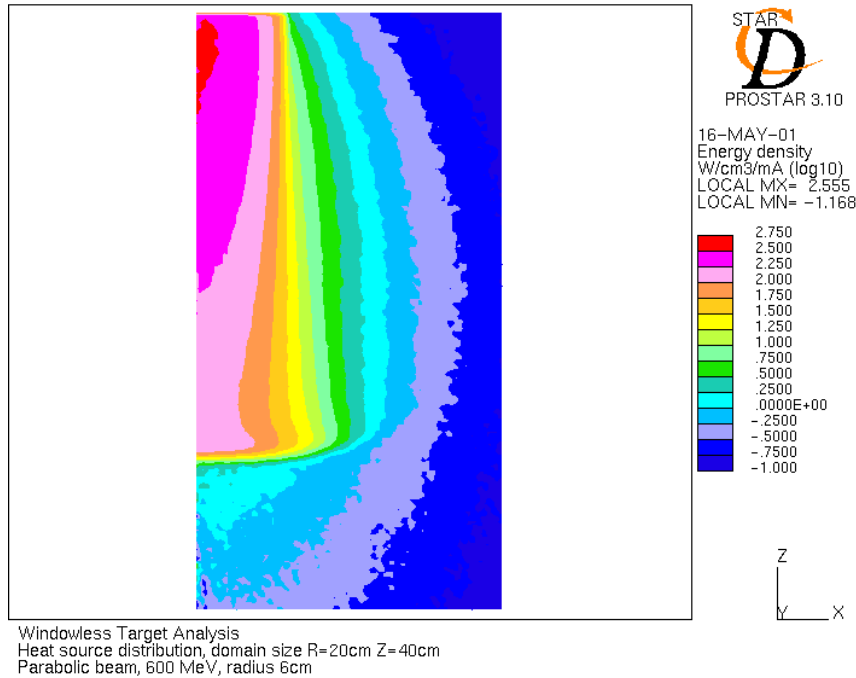


Figure 1 Heat source density distribution coming from the neutronic Fluka software. The density is for 1 mA and is given in logarithm scale to appreciate the dispersion effects. The left border is symmetry axis and the beam (6 cm radius) is coming from top.

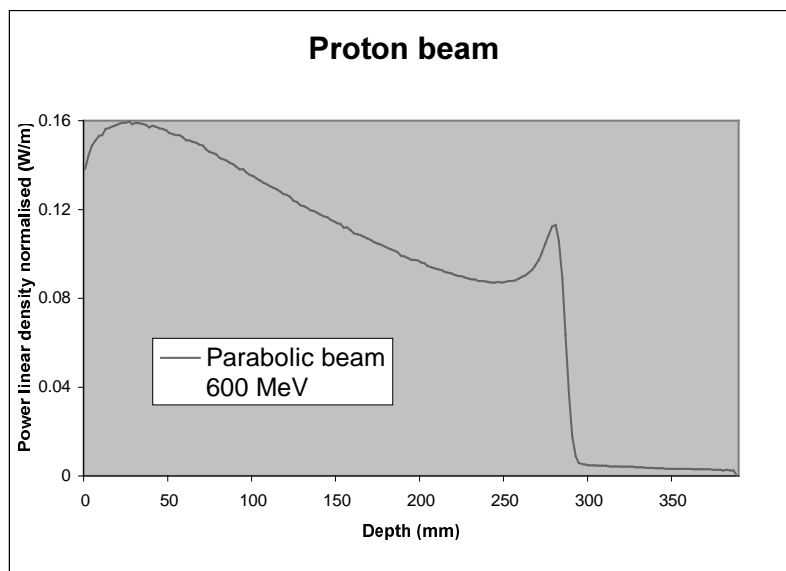


Figure 2: This curve represents the heat released by the proton beam integrated on vertical planes. One can see that the maximum is about 2 cm away from the surface and the amplitude of the Bragg pit around 28cm depth.

The radial profile is roughly preserved in the heat deposition region with a small trend to diffuse and a very small but wide dispersive queue. In Figure 3 we show a curve representing the heat source integrated over concentric cylinders. This is useful to visualize the relative heat source to the area under the curve.

Proton beam

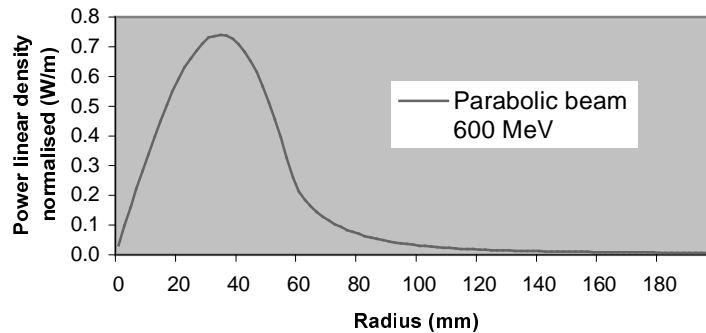


Figure 3: This curve gives the integration over concentric cylinders of the heat release shown in Figure 1. The area under the curve is proportional to the total power released inside a cylinder of a given radius. The surface under the curve right to radius 60 mm gives therefore an idea of the beam radial dispersion. Moreover, to absorb 95% of the heat source the beam region should contain a cylinder about 80 mm wide.

The deviations from the main heat deposition profile can be neglected in a first approach but should be kept in mind. The shape of the heat deposition source S can therefore be described by the formula:

$$S(r,z) = S_{\max} (1 - r^2/R^2) * (1 - 0.5 z/Z) \text{ for } z < Z \text{ and } r < R.$$

We take $Z = 30 \text{ cm}$ (z is the depth) to take weakly into account the Brag peak.

Integrating S over the whole given cylinder, we get $S_{\max} = 8/3 * Pow/\pi R^2 Z \approx 2000 \text{ W/cm}^3$.

If we integrate S over the vertical centreline and over a straight centred surface line, we have:

$$\int_0^Z S(0,z) dz = 3/4 * Z S_{\max} \text{ and } 2 \int_0^R S(r,0) dr = 4/3 * R S_{\max}.$$

Being Z much greater than R , the vertical line receive much more heat than the horizontal one.

We now look at the horizontal distribution of the heat source. Integration an horizontal straight line distant Y (with the usual convention $r^2 = x^2 + y^2$) from $r = 0$ gives:

$$Hline(Y,z) = \int_{y=Y} S(r,z) dx = Hline(0,z) * (1 - y^2/R^2)^{1.5}.$$

As shown in Figure 4, this curve is more concentrated around 0 than the parabolic curve it is derived from.

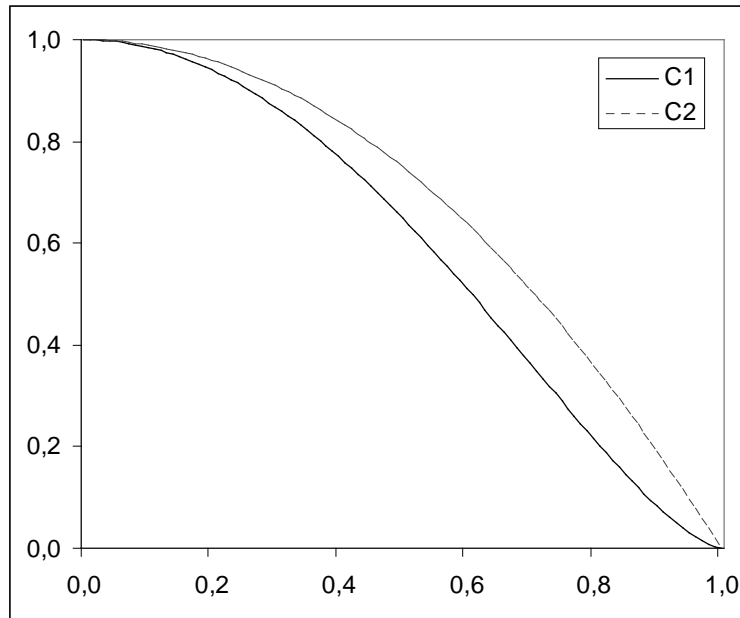


Figure 4: Curve C1 is $z = (1 - y^2)^{1.5}$, while curve C2 is $z = 1 - y^2$.

These considerations will be used to set the flow characteristics.

3.4 Flow properties

The temperature difference (in mean) between the inlet flow and the outlet flow is:

$$\Delta T_{io} = Pw / m / C_p = 2545000 / 150 / 146.5 = 115.8 \text{ K.}$$

We can notice that ΔT_{io} is not so far from $\Delta T_{max} = 150 \text{ K}$. So a uniform temperature out of the beam deposit region is a good conservative objective allowing for small deviations of the analytical derivations.

We are investigating the characteristics of an horizontal flow with straight streamlines (at least in the heat deposit region) which should, in a first approximation, give rise to a uniform outflow temperature. The streamlines velocity must be proportional to heat received and thus, supposing a flow going in the x direction, follow a profile of the form:

$$(1) v(y,z) = V_{max} * (1 - y^2/R^2)^{1.5} * (1 - 0.5 z/Z).$$

and V_{max} is found from the equality: $\rho C_p \Delta T_{io} V_{max} = 4/3 * R S_{max}$, that is $V_{max} = 0.92 \text{ m/s}$.

Note that the temperature requirement is quasi surely unmatched if the effective maximum velocity is less than $V_{max} * \Delta T_{io} / \Delta T_{max} = 0.71 \text{ m/s}$.

For the central cross-section of $16 \text{ cm} \times 30 \text{ cm} = 480 \text{ cm}^2$ the mean velocity is about: $V_{mean} = 0.31 \text{ m/s}$.

In the following, we present some means to approach such a flow configuration.

4 Flow tailoring

Our objective is now to tailor the flow according to equation (1). Nevertheless, we keep in mind the existence of the dispersive beam queue and the constraint on the pressure drop. We split the analysis into three sub-problems.

- Flow horizontality
- Vertical flow tailoring
- Horizontal flow tailoring

4.1 Flow horizontality

We want the flow to be horizontal in the beam deposit region. An easy way to obtain this feature is to split the flow in several sub-channels as shown in Figure 5.

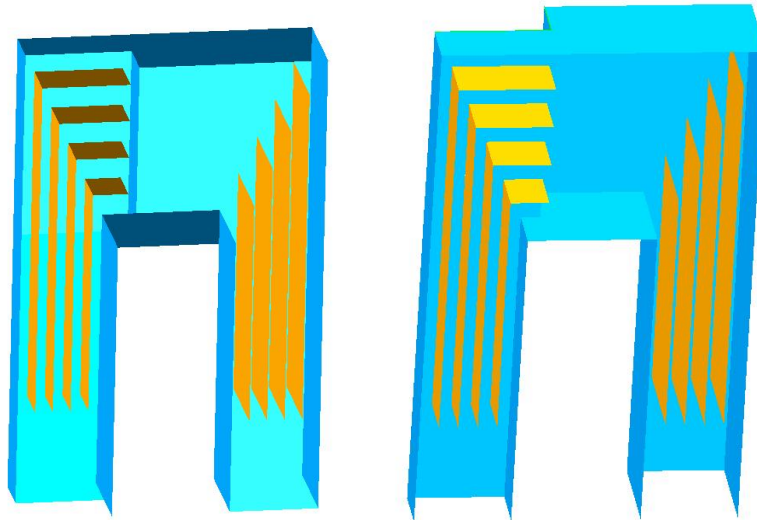


Figure 5 Sketch of a windowless channel. Half of the channel is shown. The flow rises from the left, is bent horizontally by the flow separators and goes down on the right side. In this case, the inlet is restricted laterally to concentrate the flow in the centre region

In the case of sub-channels separated also in the beam region, to get a good horizontal flow we must:

1. Minimise $|h/l - 1|$, where h is the height of the sub-channel in the centre region and l is sub-channel width in the rising region.
2. Increase the sub-channel number.
3. Maximise the horizontal separator length.

To control the pressure losses, we must:

1. Minimise $|h/l - 1|$
2. Limit the sub-channel number (to lower the friction losses).
4. Smooth the elbows, maximising the curvature radius.

In the case of similar sub-channels as in Figure 5, we have $|h/l - 1| = Z/L - 1$ where L is the width of the entire rising channel. To insert a rectangular channel not too thin in a 52 cm diameter cylinder, we can count on about 48 cm. Taking off the 12 cm for the beam region and splitting the rest in 2 for the inlet region and the outlet region, it comes a maximum value for L of $L_{\max} = 18$ cm and $Z/L_{\max} = 5/3$. But in this case, there is no room to curve smoothly the innermost sub-channel and the elbow may result excessively resistive. The perfect horizontality is not critical on the border of the heat deposition region and some place can be retrieved to curve the innermost sub-channel. The problem linked to a high Z/L ratio and a small curvature radius are illustrated in (). Essentially, a vortex may develop in outlet of the curve which increases the friction losses but above all may entrap some heated fluid with the risk of reaching undesired temperatures.

Some interesting results have already been reached on this basis and it is an on-going line of optimisation.

Full optimisation of the Z/L ratio can be achieved at the cost of some added geometrical complexity.

In fact, equation (1) can be written independently for each z -level. That is, the direction of the flow may be different at different depth. In the precedent case, the rising part of the channel is included in a given limited angular sector and there is room to put another rising part rotating, say, 45 degrees as illustrated in Figure 6 and Figure 7. If the central part is located at a different height, then both channels can easily coexist. Up to 4 channels can be inserted in this way without difficulties. A target based on this concept is shown in () with 4 rising and 4 down-coming regions occupying the entire external annular region of the cylinder. In this case, the solid separators have been taken off in the central region.

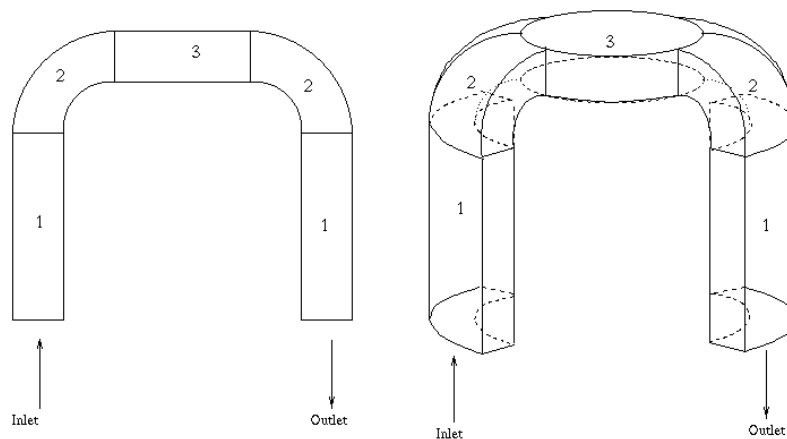


Figure 6 Conceptual design. A channel can be split in 3 zones: the vertical channels, the elbows and the central region. This is illustrated on the left in a plane context and on the right in a cylindrical context.

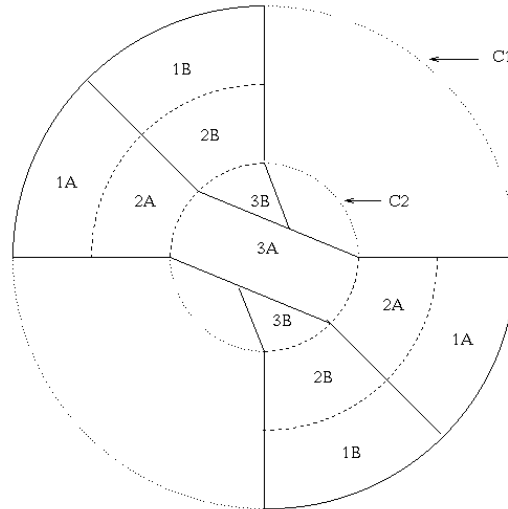


Figure 7 Conceptual sketch. Top view of the region occupied by two separated channels. The channels must be enclosed inside the delimiting circle C1. Regions 1 and 2 of channel A and B should not overlap while, being at different height, regions 3A and 3B can freely overlap as long as they stay inside the delimiting circle C2.

Using 2 channels, the aspect ratio Z/L can be put to 1 (considered here as optimum). With 3 or 4 channels, additional place is gained to curve smoothly the elbows. It should be noted that this method of channel multiplication and segregation is orthogonal to the splitting in several sub-channels and both methods can be used together according to other constraints.

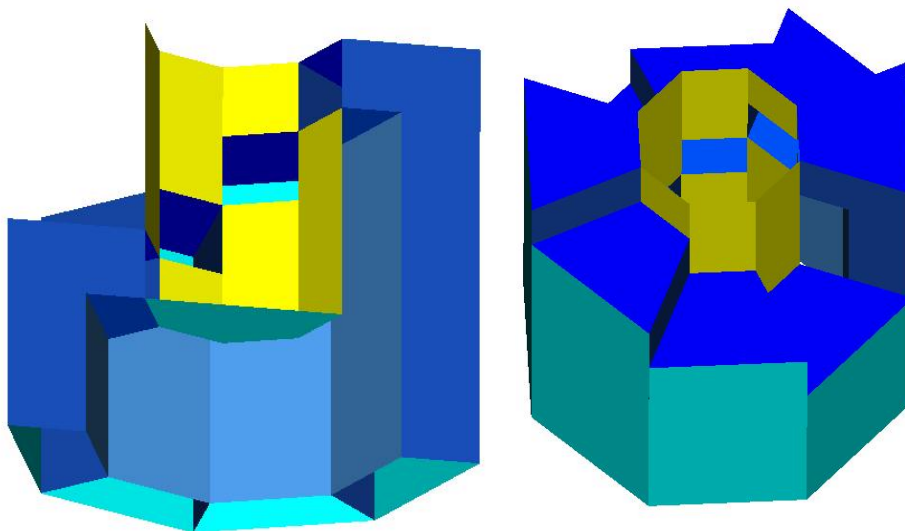


Figure 8 Windowless target with 4 separated channels in inlet and in outlet.

4.2 Horizontal flow tailoring

According to 4.1, we suppose to dispose of an horizontal flow, at least up to a reasonable distance of the centre. To take into account the beam dispersive queue, we require a 2 cm security gap and each channel must encompass a centred cylinder whose radius is at least 8 cm. The flow in the additional 2 cm may be low but preferentially not nought and with no re-circulating part (same risk than high Z/L ratio). On the remaining 6 cm, we want the flow velocity to be close to equation (1). On another hand, having the widest rising region is best suited to limit pressure losses.

For simplicity we only consider channels which are symmetrical in confront of the cylinder axis. Each (half-)channel can be split in three different regions as illustrated in Figure 6. First is the region where the flow rises vertically, then the elbow where the flow is (hopefully) curved horizontal, and finally the central plane region where the flow is heated. As shown in Figure 7, the first two regions are constrained in an angular sector with a given opening, so that other channels can be inserted. On the contrary, the third regions are at different height for each channel and therefore can encompass the all or any part inside the limiting circle.

There are no clear indication that region 1 and 2 should not occupy all the space at disposal. Region 3 must encompass a circle whose radius is at least 8 cm and there is no need for much more, the heat released out of this range being expected to be removable by simple thermal conduction. We will therefore tend to limit the radius of the included circle between 8 and 10 cm.

To get a profiled velocity field, one can throttle the channel before arriving to the heating region. This is naturally done in the cylindrical reference frame (region 1 and 2) but can prolonged in region 3. Region 2 and 3 have also to connect smoothly to avoid re-circulation at the corners. This is illustrated in Figure 9.

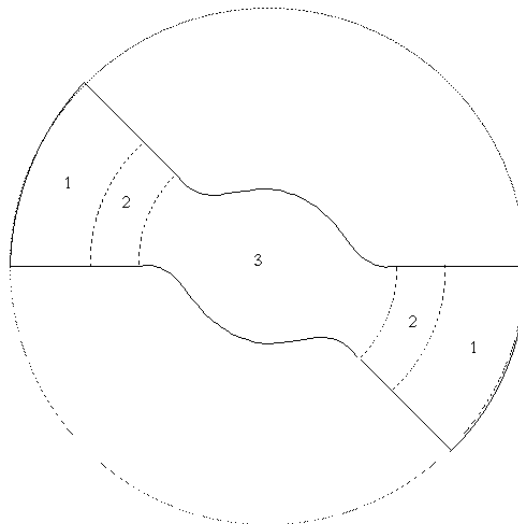


Figure 9 Top view of a channel. Regions 1 and 2 are enclosed in a sector and naturally concentrate the flow in the centre. This feature can be propagated in region 3 and a smooth connection can also be done.

From a geometrical and meshing point of view, region 1 is the extrusion of a rectangle in cylindrical reference frame. Region 2 is the extrusion of an annular sector in the same reference frame. In Figure 10, we show a geometric transformation allowing to construct region 3 with a conform connection to region 2. A mesh assembly based on these principles is shown in Figure 11

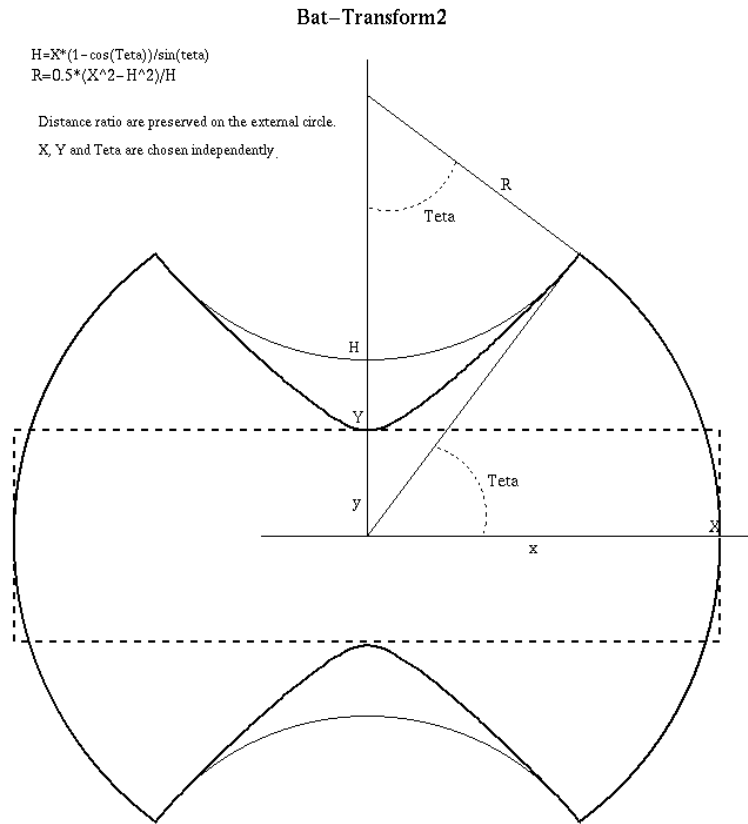


Figure 10 Conceptual design of a geometrical transformation modifying the dashed rectangle into the bold continuous perimeter. This transformation is very useful to realise a smooth connection with a coaxial angular sector of fixed opening while keeping control of the throttling at the centre.

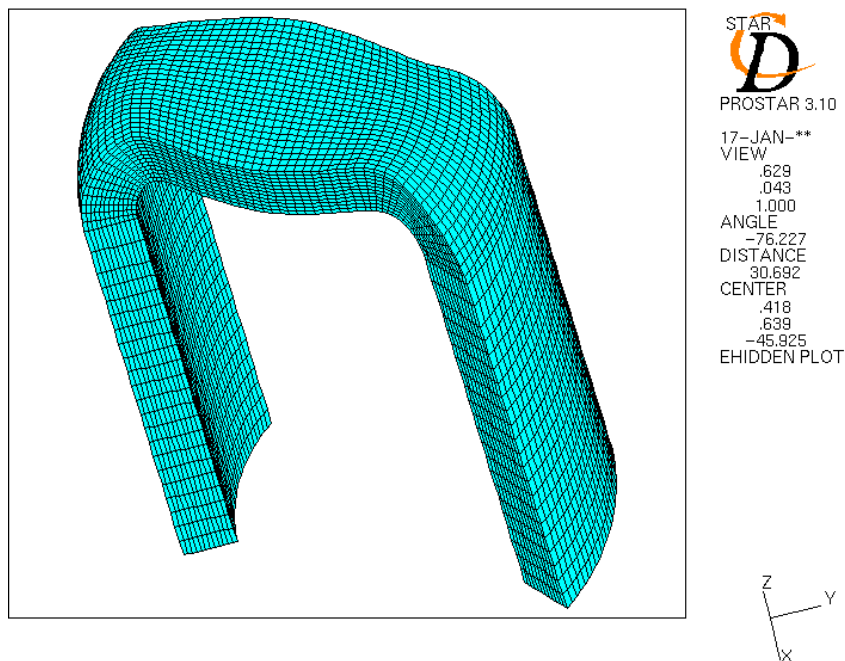


Figure 11 Mesh assembly connecting smoothly two rising coaxial angular sectors to a flat central region. This geometry has the stering properties described in Figure 7.

The throttling can be enhanced by allowing a smaller angular sector. If too strong, it can generate vortices on the borders which are to be avoided, being the potential seed of excessive temperatures. That is why it could be worthwhile considering the adjunction of a non-uniform pressure drop grid slowing down the flow preferentially on the borders. The grid may be placed at the centre of the throat.

4.3 Vertical flow tailoring

The vertical flow tailoring can be done by use by the adjunction of pressure drop grids on each channel or sub-channel where the velocity is not the highest. If the segregated multi-channel technique is used, each channel (and even sub-channel) has roughly the same global pressure loss coefficient X_0 mainly caused by the 2 elbows, the 2 throats and the optional differentiating grid. According to [2], to get an homogeneous outflow temperature, the mean velocity in each channel must be proportional to the mean heat to the heat released in this channel. To equilibrate the pressure, it comes out:

$X_i = X_0 (S_1/S_i - 1)$ where X_i is the additional pressure drop coefficient needed in channel i and S_i is the heat source in this channel with its maximum in the first channel. An analysis of the stability of this configuration can also be found in [2].

4.4 Channel separation

In 4.1, 0 and 4.3, we have mainly considered the case of channels and sub-channels connected exclusively through their extremities from on part and the other of the spallation region. At this point, several options can be investigated:

1. No change: this is an alternative multi-window beam target.
2. The top channel has a free surface: this is an hybrid “windowless-multi-window “ beam target. While a priori quite complex, it has a few interesting features:
 - The free surface flow has a clearly horizontal channel configuration.
 - The intermediate windows are cooled both sides and heated less.
 - The intermediate windows do not withstand heavy loads.
 - Cracks in the intermediate windows are not critical.
 - The free surface paradigm can be treated separately.
3. All channels are connected in the central region, by removing all the walls in a central cylinder of radius at least 6 cm. In this case, some additional work must be done on the pressure losses. In effect, the pressure drop must equilibrate for each (sub-)channels both between the inlet and the centre but also between the centre and the outlet. In other words, to avoid mass transfer between channels, the mass flow rate must be the same both sides from the spallation region and we must consider the adjunction of a second set of grids to reach the equilibrium. Some tri-dimensional effects are expected from the contact of flows with different velocity and eventually a different flow orientation. These effects are expected to not critically alter the flow features but must be carefully looked at.
4. All channels are connected, digging the same 8 cm radius cylinder, but keeping the top surface closed. This is another window type beam target. For our concern, it is only a convenience

allowing to investigate separately the free surface problematic and the effects of the central connection.

5 Optimisation past history

The first type of windowless channel to be studied has an axial-symmetrical configuration (ref Myrrha). While conceptually very simple, it presents strong technical difficulties, mainly due to the presence of a theoretical stagnation point at the symmetry centre corresponding to a highly turbulent re-circulation region in the experimental settings. The problem has been conceptually solved at the cost of rotating the proton beam around the re-circulation zone. On the other hand, the free surface chaotic structure is very difficult to investigate and reproduce with CFD tools.

Mainly because in the EADF conception, a great effort is done to avoid mechanical mechanism and encourage passive systems, it has been decided to investigate an alternative windowless target configuration, namely a windowless channel target. In the following, we trace back and analyse previous attempts which have lead to the actual understanding of the problematic.

5.1 Single channel optimisation trial

At the beginning, we hoped to find a satisfying result from a very simple base configuration, as shown in (), where a rectangular channel is connected to a rectangular riser at one end and to a rectangular down-comer at the other end. The parameters were the three dimensions of the channel, the width of the riser connection, the width of the down-comer connection and the beam radius. A typical flow configuration is given in ().

The first information was that the steady-state simulations almost never converged. Further transient simulations confirmed that the flow was unlikely to reach a stationary configuration. Varying the parameters, we got basically 2 kinds of flow configuration.

The first flow configuration is illustrated in (). The flow globally curve around a big central vortex. Part of the vortex is inside the heated region and so a maximum of the temperature is reached inside the vortex. The vortex is in-stationary showing an evolution in size, temperature and localisation. The vortices always showed a tendency to rise while growing and it was not possible to stabilise it safely out of the heated region.

The second flow configuration has been found out, trying to kick off the vortex from the heated region. When the surface streamlines are too weak, the temperature at the surface rises more than in the bulk flow and the buoyancy force tends to impede the heated fluid to go down the down-comer effectively slowing down the fluid which therefore is heated more. A critical instability develops in which a very hot re-circulating or dead zone expands from the free surface. This configuration is illustrated in (), noting that the numerical simulation does not take any vaporisation or boiling effects into account.

The hot vortex flow can be considered in a way satisfying, because the main requisites are substantially met and even if the vortex varies, it stays in the bulk flow. Nevertheless, while the typology of the flow is reasonable we feel that the flow pattern is very sensitive to the numerical approximations relative to the turbulence model. The main fear is that in a real flow, the hot vortex may occasionally slip off its central position, rise up by one side under the buoyancy force and start an instability leading to the second flow configuration.

The conclusion of these works was that we had to control much better all the streamlines and find out a basically stable satisfying configuration.

The free surface on top of the channel has been simulated as a slip wall.
 Buoyancy has been taken into account.
 NSE solved for mass, momentum and energy.
 Parabolic proton beam: 600 MeV, 12 cm diameter, 6.62 mA intensity.
 The proton beam has been simulated as an energy source.
 Coolant: liquid Pb-Bi eutectic.
 Mass flow rate: 200 kg/s.
 Inlet temperature: 300 °C.

5.1.1 first analysis

Modelling features:

- turbulence model: K-e/RNG,
- numerical scheme: upwind,
- convergence algorithm: SIMPLE.

The cooling water flowing around it is simulated imposing a temperature of 20 °C on all the target walls.

The spallation heat is introduced as a source term in the lead energy equation.

The channel is 45 cm long and 16 cm wide.

For symmetry reasons, only half channel has been simulated.

A structured mesh was used (see figure 1). The total number of elements is 31600. Steady-state and transient calculations were performed using the SIMPLE and PISO algorithms respectively. Some convergence problems were reported.

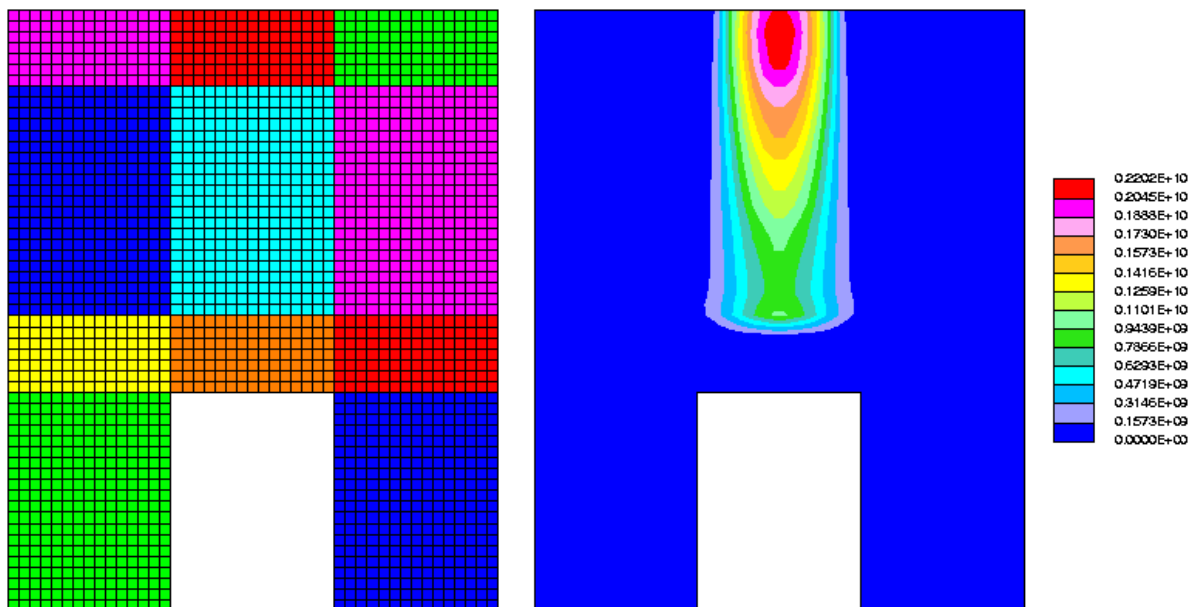


Figure 1: mesh and fluka

Test Case	Channel depth	Inlet width	Outlet width	Maximum temperature on free surface (°C)	Maximum bulk temperature (°C)
A1	30	10	10	425	1397
A2	35	10	10	439	1445
A3	40	10	10	450	1282
A4	45	10	10	457	854
A5	35	15	15	608	463
A6	37	13	13	574	579
A7	38	12	12	585	1093
A3	40	10	10	450	1282

Table x:

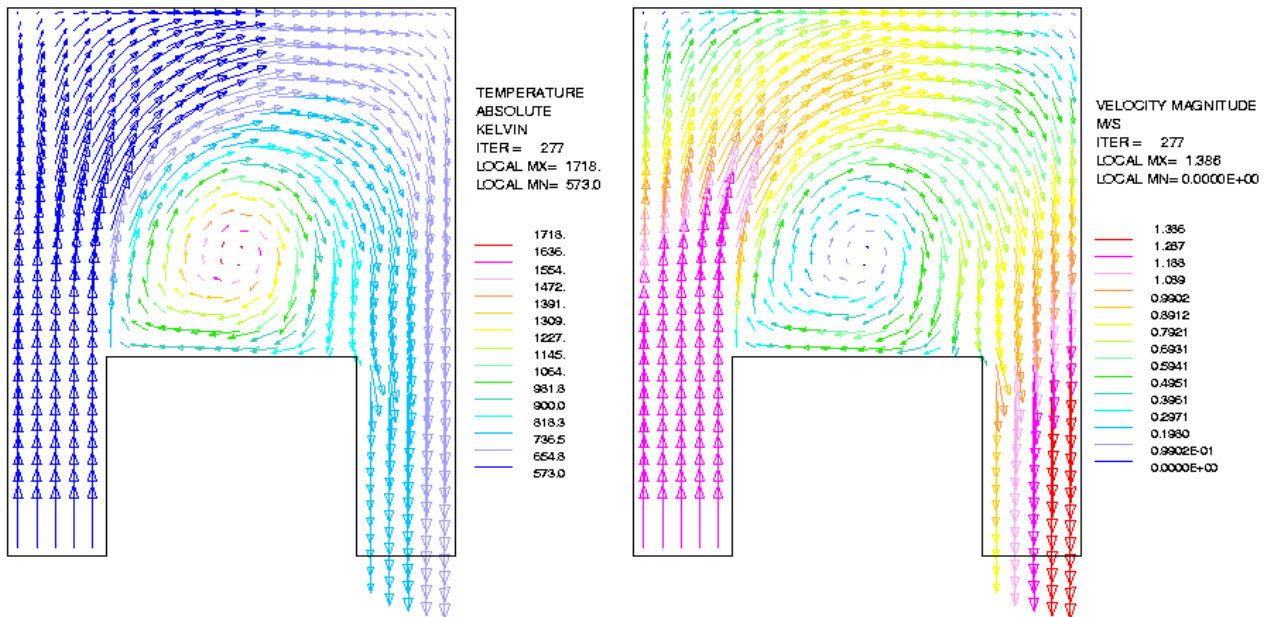


Figure x: 351010 temp e vel

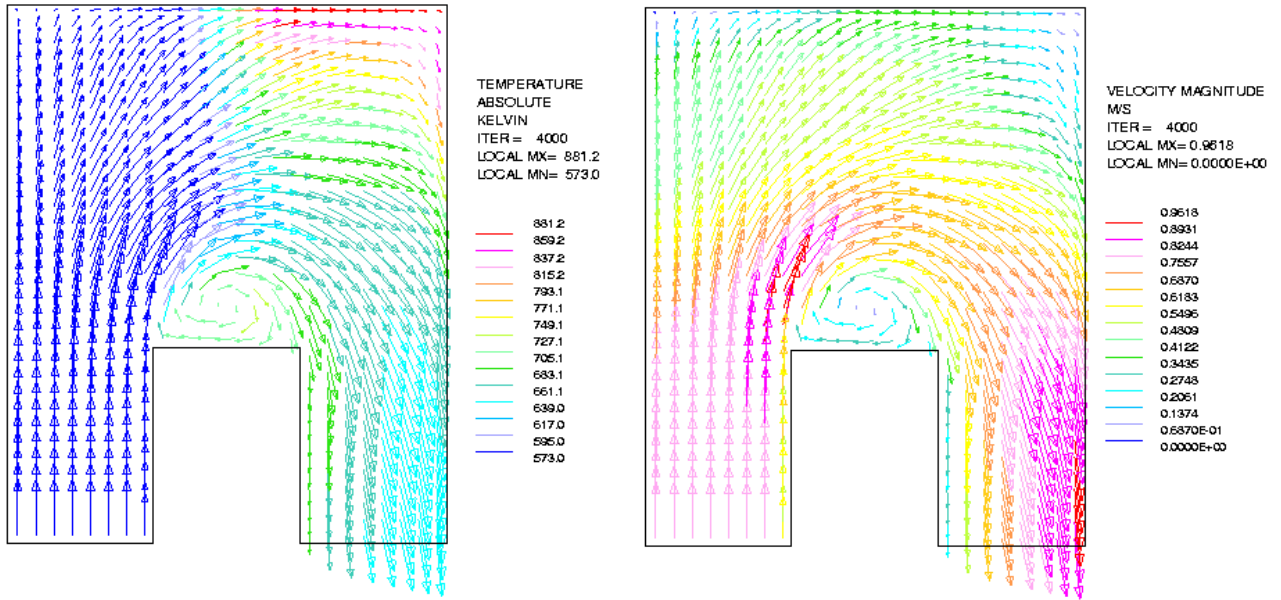


Figure x: 351515 temp e vel

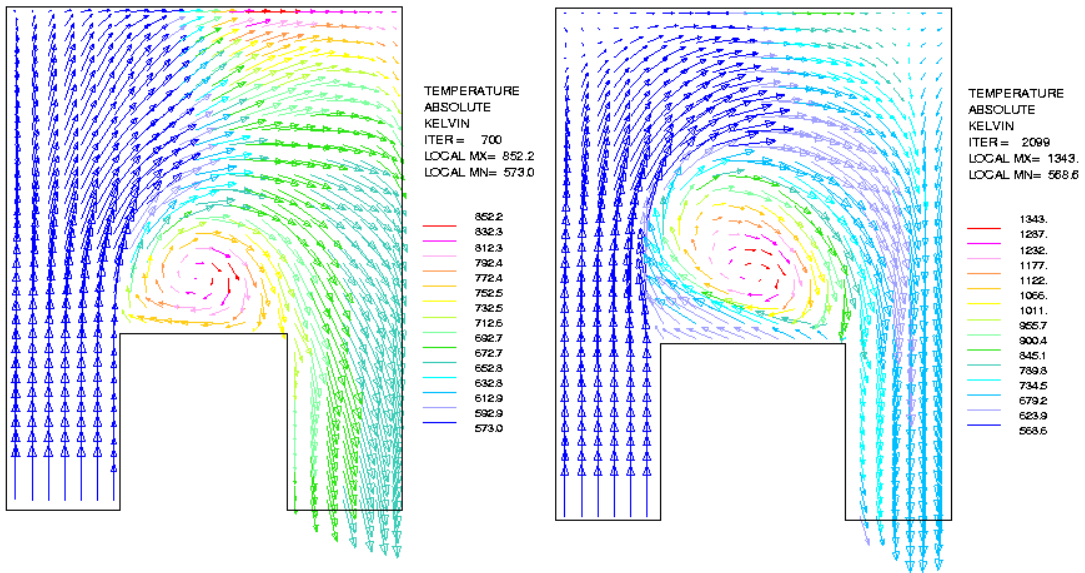


Figure x: 371212 e38 12 12

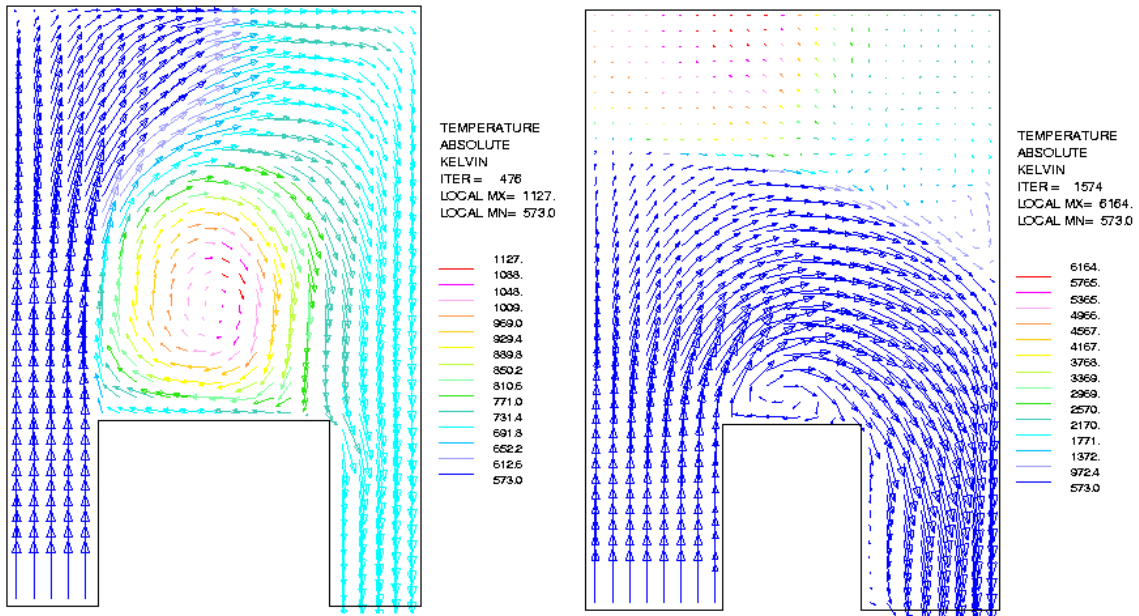


Figure x: 451010 e 451515noconv

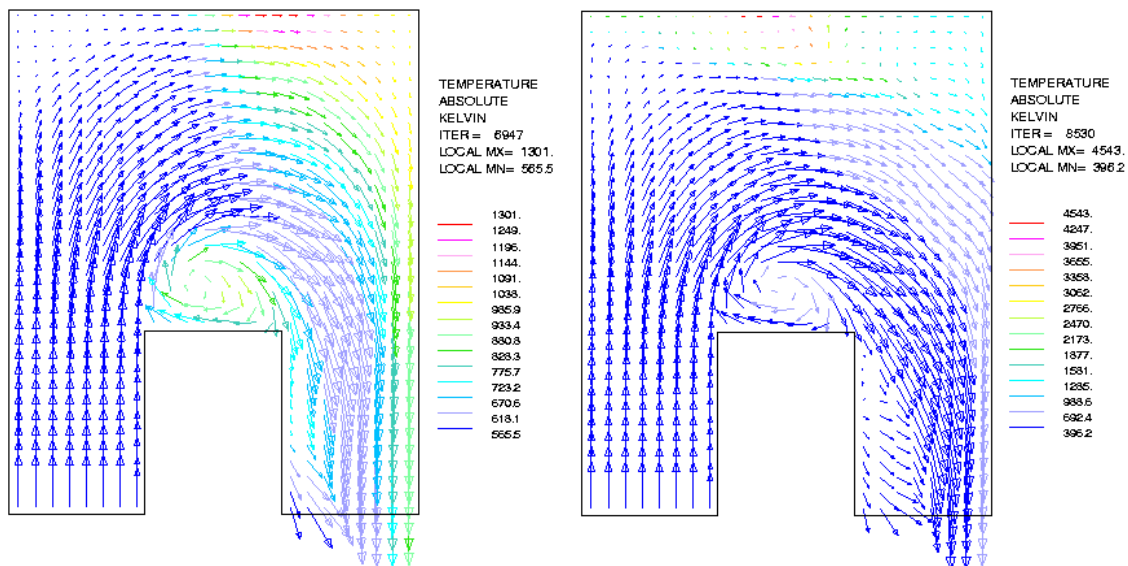


Figure x: 351515noBconv, 351515 Bnoconv

Partial conclusions

From these results, it seems that the maximum temperature increase can be kept under 300 °C (with a mean increase of 100 °C).

Further improvements could be obtained, even introducing new parameters in the problem.

However, the following considerations should be taken into account:

Numerical convergence of the simulation failed in a number of other cases.

This behaviour is strongly dependent on the numerical scheme and is widely encountered for high order (more accurate) numerical schemes.

Under certain parameter values the flow generates an upper hot stagnant region.

This behaviour is caused by buoyancy forces and leads to unacceptable temperatures (boiling).

Buoyancy forces are a key feature of the flow (in-)stability and must be absolutely taken into account.

Low-order numerical schemes must be avoided because the numerical diffusion damps the buoyancy effects.

More geometrical optimisation has to be done, paying special attention to the shape of the inlet and of the walls.

Free surface

A measure of the error caused by replacing the free surface with a solid wall is given by the pressure variation on the surface.

Case	A1	5.1.1.1.1 2	A3	A4	A5	A6	A7
SurfaceΔP [Pa]	4370	3523	3088	2832	780	1093	977

Table x:

If this value is too high, the numerical simulation can completely non-consistent.

The previously described flow separation should be avoided or at least strongly minimised, in order to avoid these problems:

the re-circulation zone is strengthened by the buoyancy force;

the surface shape is usually non-stationary and we are not yet able to couple the proton beam with a moving domain.

Conclusions

The first results are encouraging but may be misleading.

More geometrical optimisation is still to be done.

High order schemes are compulsory.

Buoyancy effects must be accounted for.

The free surface analysis is very complex but it could be damped if the geometrical optimisation minimise the surface deformation.

5.1.2 seconda serie

Modelling features

5.1.2.1 The mesh is refined

Grid: 54900 elements, 62524 nodes (transient model: about 216000 elements, 200000 nodes)

5.1.2.1.1.1 Half size model

Use of a classical turbulence model: Chen K- ϵ

Numerical scheme: QUICK.

Convergence algorithm: SIMPLE. Transient: 20 s with constant time step of 0.002 s.

Analysis constraints

Coolant: liquid Pb-Bi eutectic.

Mass flow rate: 200 kg/s.

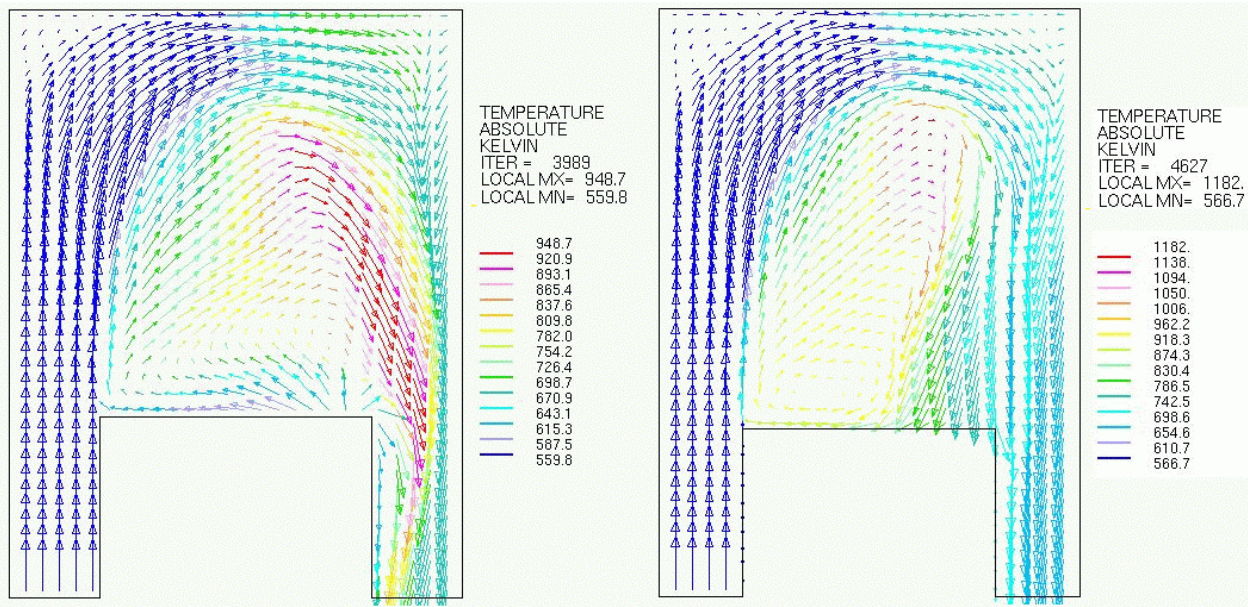
Inlet temperature: 300 °C.

Parabolic proton beam: 600 MeV, 12 cm diameter, 6.62 mA intensity.

Channel: 50 cm length, 16 cm width.

Test Case	Channel depth	Inlet width	Outlet width	description	Maximum bulk temperature (°C)
B1	45	10	10		-
B2	50	10	10		-
B3	55	10	10		-
B3T	55	10	10	Transient analysis	906
B4	60	10	10		
B5	55	10	10	Inlet guide 20 cm height	-
B6	55	10	10	Inlet guide 30 cm height	-
B7	55	10	10	Outlet guide 30 cm height	-
B8	55	10	10	Outlet guide 40 cm height	-

Table x:



5.1.2.1.1.2 Figure x: 450 e 500

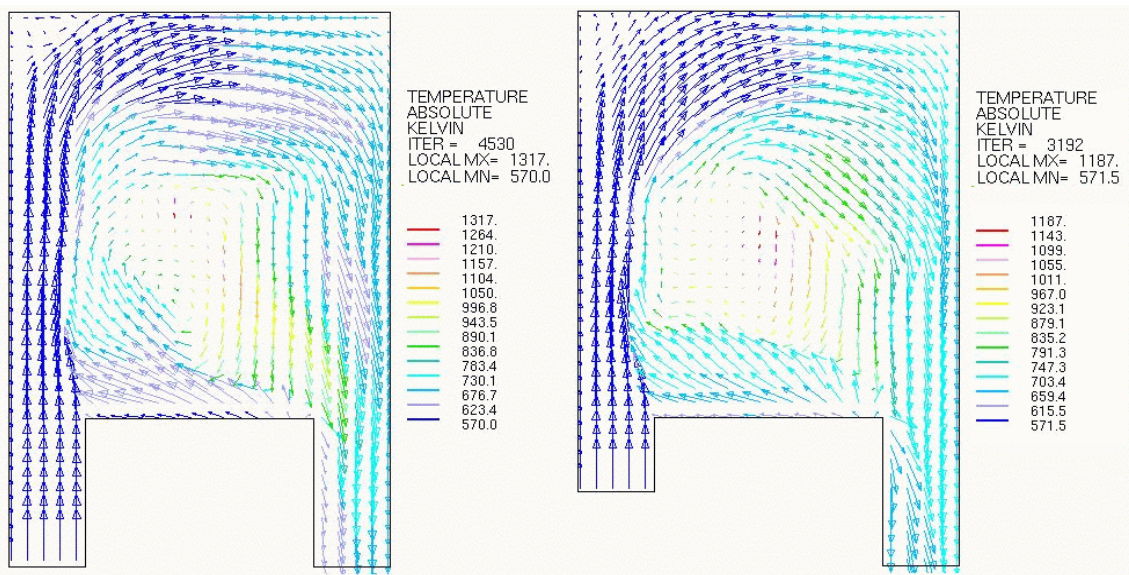


Figure x: 550 e 550T

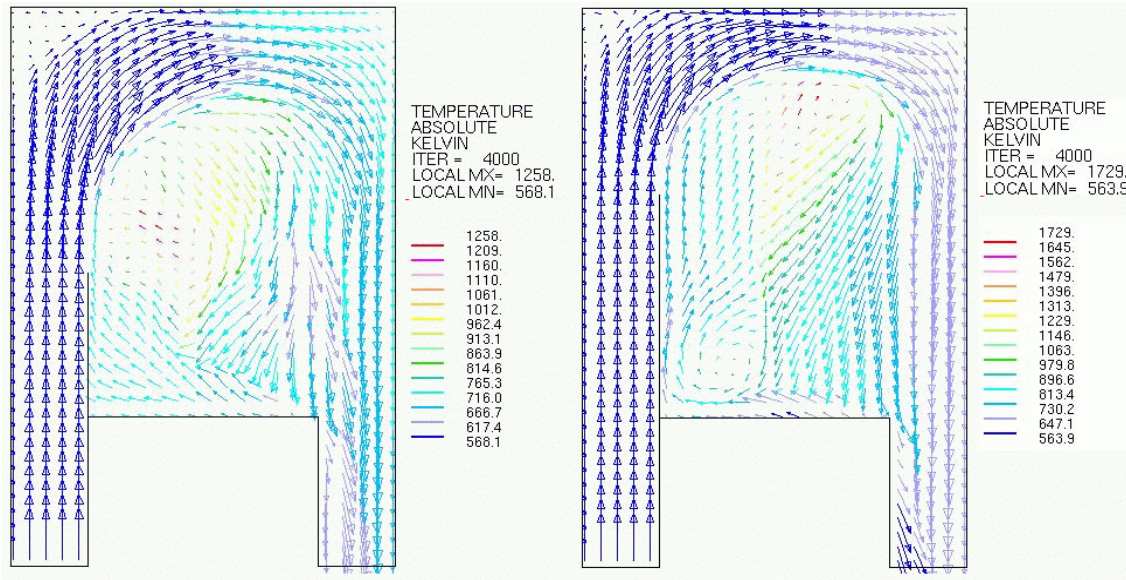


Figure x: 550sx200 e 550sx300

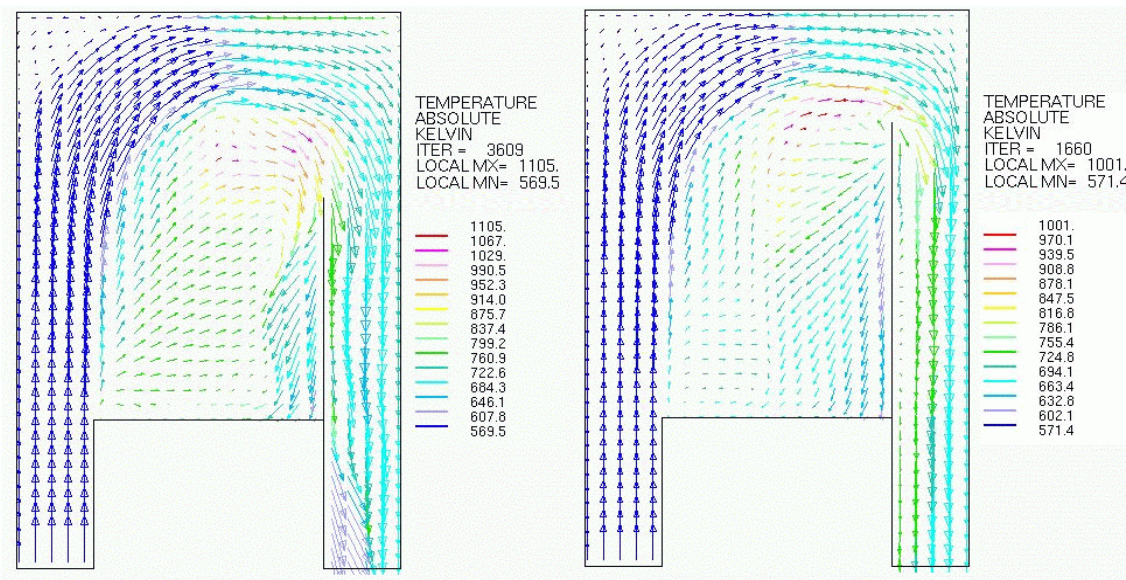


Figure x: 550dx300 e 550dx400

5.2 Optimisation of the channel splitting

The easiest way to guide the flow is to inset flow-guides. In the following we briefly illustrate a first optimisation process. The scope of the optimisation was exclusively to lower the maximum temperature both in the bulk and at the free-surface. The mean was the insertion of flow guides in the riser and eventually in other parts of the target.

As shown in Figure 12, the insertion of guides in the riser and symmetrically in the down-comer so as to distribute equally the flow through the different levels resulted in a very nice symmetrical flow, quite stable but with an unacceptable temperature in the bulk.

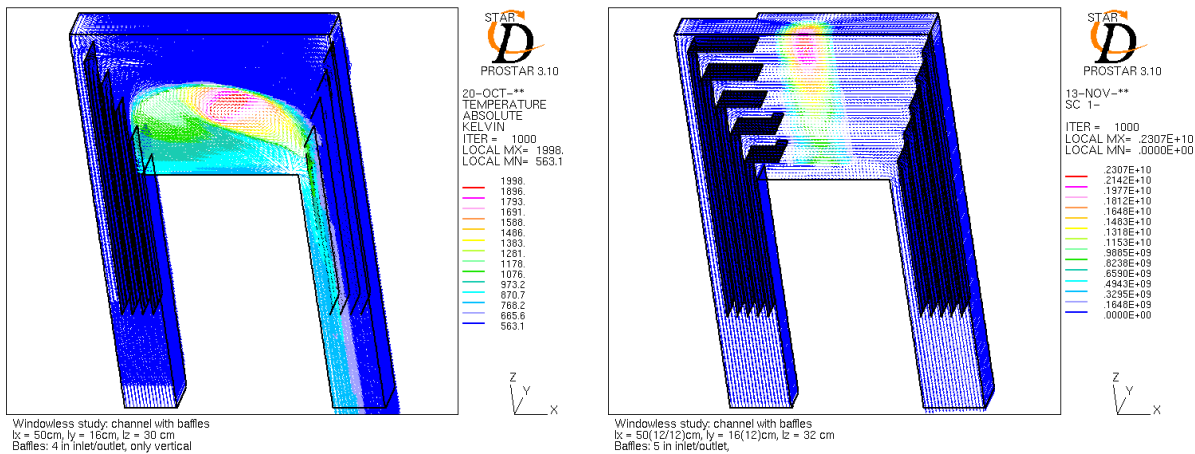


Figure 12 On the right, channel with baffle insertion to distribute the flow. Front view is the symmetry plane. There is very hot central region (up to unphysical values) where the flow is re-circulating. On the left, apart from geometrical modification, the heat source coming from the proton beam is shown.

Therefore, we have completed the guides with an horizontal part to kill the hot spot. The result is shown in Figure 13 and is extremely encouraging. In the second case, the greater number of guides has limited the small vortices downstream of the elbows. We can notice that the fluid is hotter in the middle of the channel and the idea was to reduce the riser width to concentrate the flow in the middle of the channel. In Figure 14, we have reduced the riser to $\frac{3}{4}$ and to $\frac{1}{2}$ width. In the first case, the result is sensibly better and in the second case we encounter the limit of the method. In effect, the maximum temperature is then located at the surface level and is caused by the creation of a vertical vortex after the enlargement.

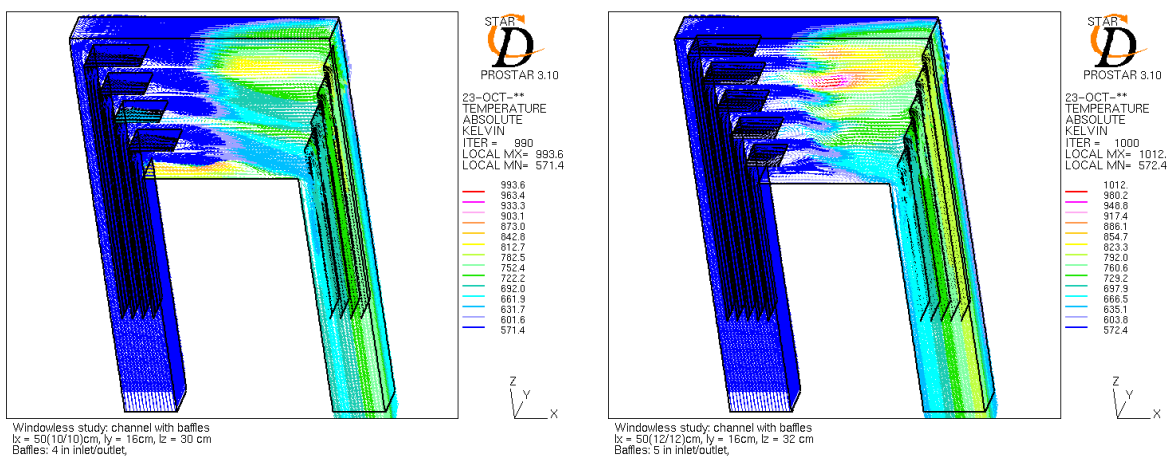


Figure 13 The insertion of vertical baffles destroys completely the re-circulation region shown in Figure 12. On the left, the hottest region is at the bottom of the horizontal part where the flow exhibit a re-circulating motion. The insertion of an additional baffle to restrict the innermost

channel, as shown on the right, solve this problem and transport the hottest point in the bulk of the channel.

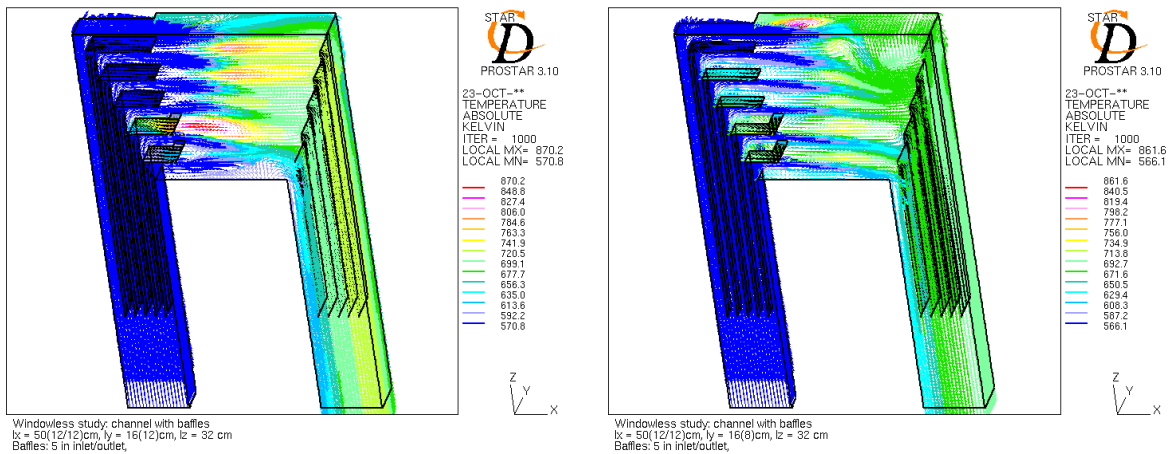


Figure 14 Effect of the restriction of the inlet width on the temperature. On the left, the inlet width is only $\frac{3}{4}$ of the channel width, and the effect is a clear temperature drop everywhere in the channel. On the right, the width is reduced to $\frac{1}{2}$, and we can see the limit of the method because the maximum temperature is now on the surface and is due to a vertical vortex downstream the enlargement.

A clear line of optimisation, at this point, is the three-dimensional shaping of the channel to smooth elbows and enlargements.

5.3 Windowless multichannel analysis

5.3.1 Modelling features

3D steady-state simulations.
Free surface simulated as a slip wall.
NSE solved for mass, momentum and energy.
Buoyancy is taken into account.
Proton beam simulated as an energy source.
Use of a classical turbulence model: K- ϵ /Chen
Numerical scheme: upwind.
Convergence algorithm: QUICK
Grid: about 110000 elements and 100000 nodes
Full size model

5.3.2 Analysis constraints

Coolant: liquid Pb-Bi eutectic.
Mass flow rate: 150 kg/s.
Inlet temperature: 300 °C.
Parabolic proton beam: 600 MeV, 12 cm diameter, 6 mA intensity.
Channel: 50 cm length, 16 cm width.
Inlet channel: 15 cm length, 16 cm width.

Outlet channel: 15 cm length, 16 cm width.

5.3.3 Results

Test Case (Type/section)	Convergence (iterations)	Maximum temperature (°C)
Asymmetric Rectangle	NO (2000)	3000
Asymmetric Batman	OK (3000)	960
Asymmetric Lucas	NO (3000)	880
Symmetric Rectangle	NO (1500)	760
Symmetric Batman	NO* (1500)	730
Symmetric Lucas	NO (3000)	850

Table x: results

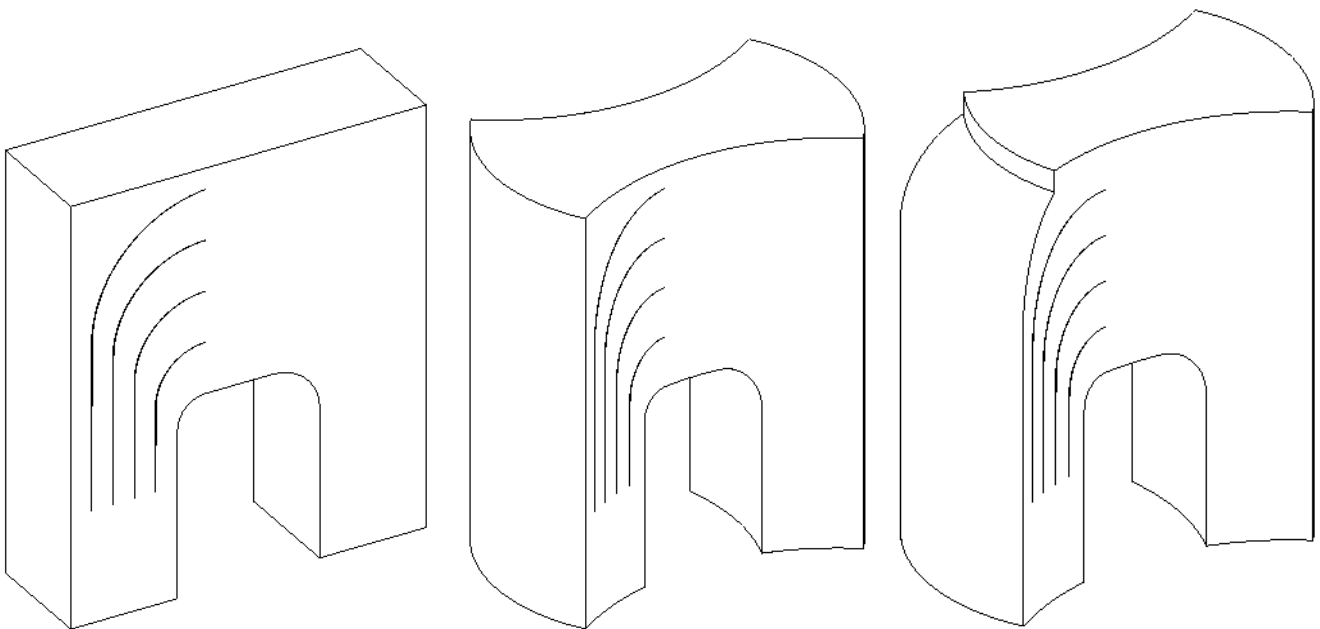


Figure x: geometry model

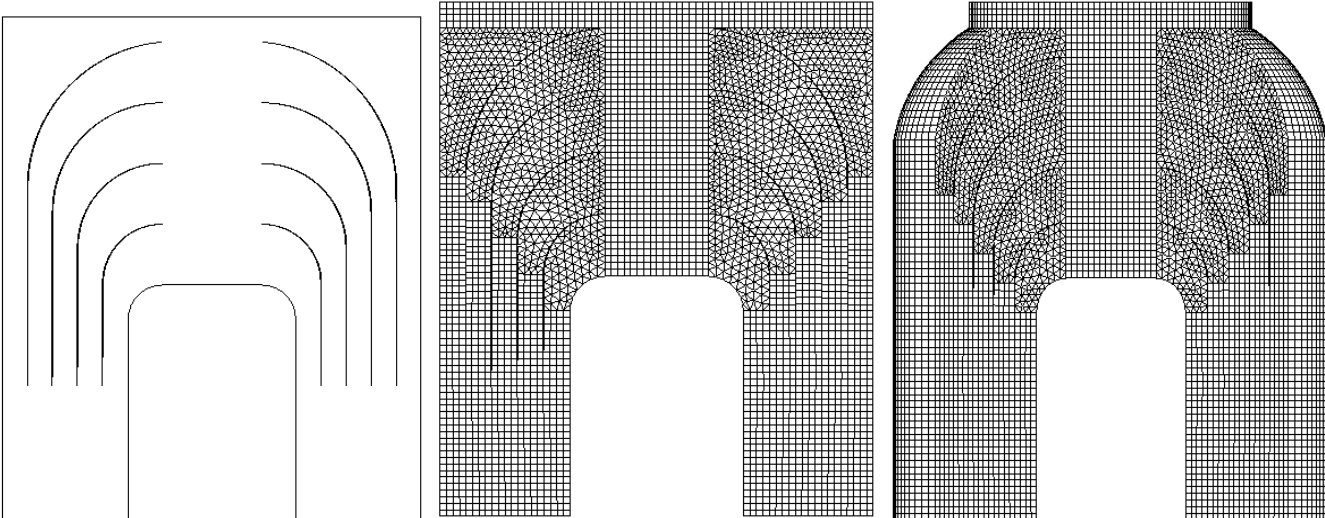


Figure x: geometry and mesh example

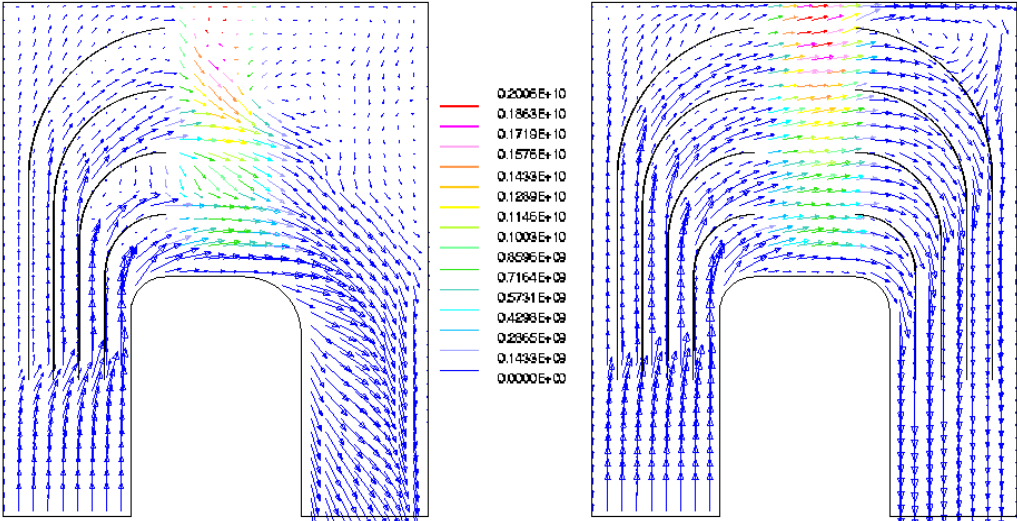


Figure x: fluka

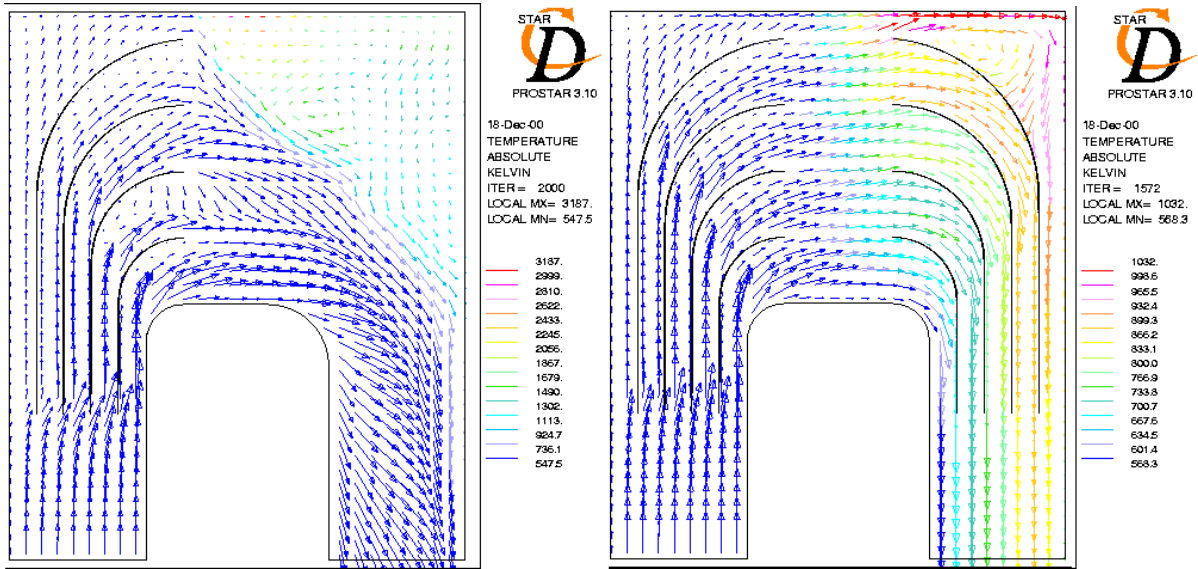


Figure x: rectangle section, inlet multichannel and inlet/outlet multi channel

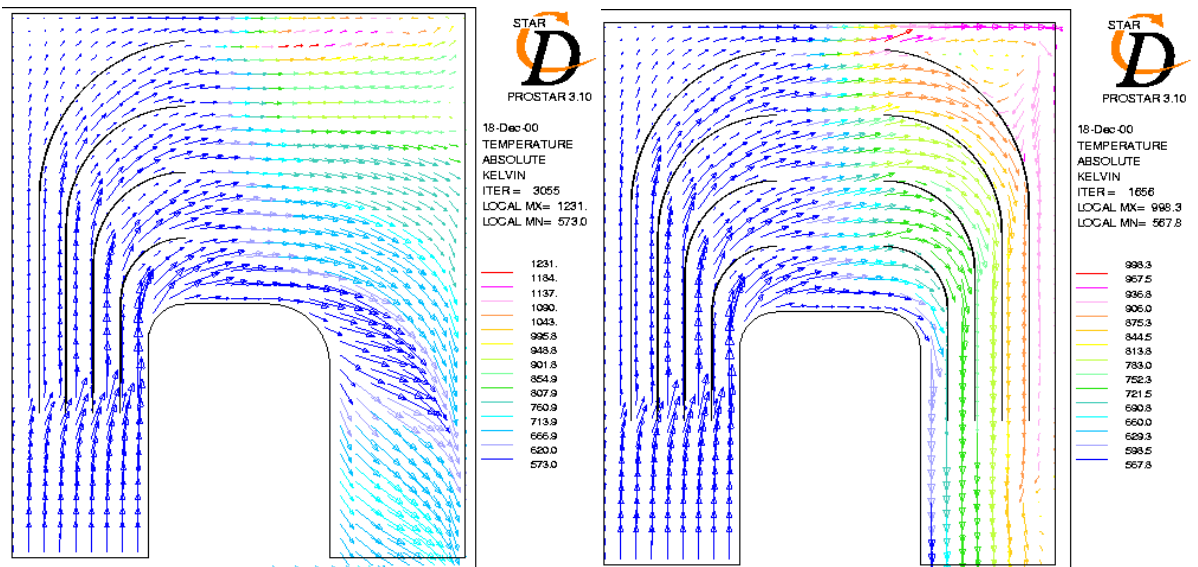


Figure x: batman section, inlet multichannel and inlet/outlet multi channel

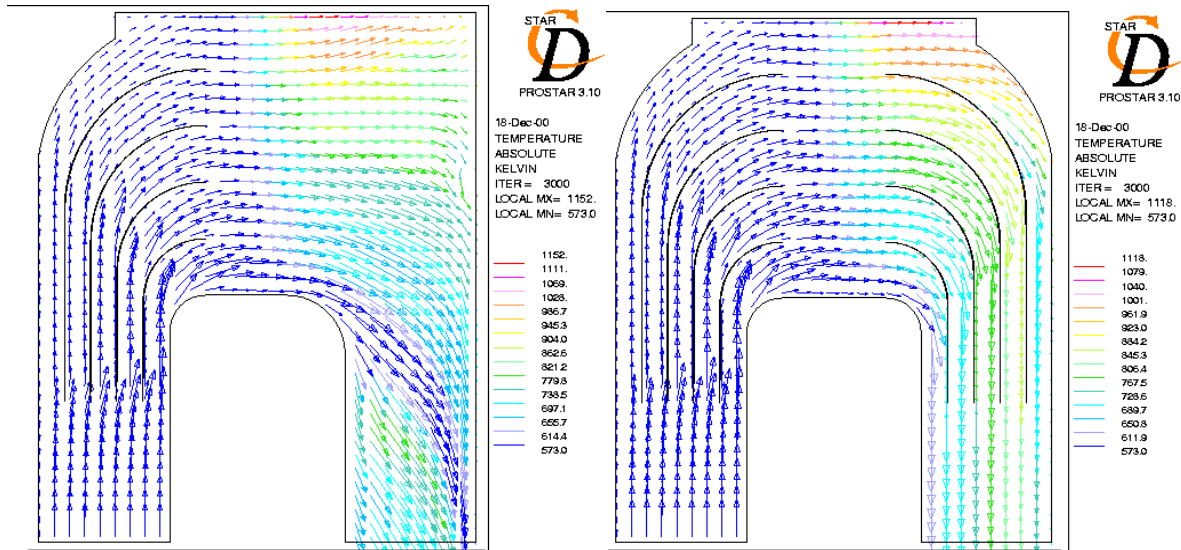


Figure x: lucasbatman section, inlet multichannel and inlet/outlet multi channel

5.4 Encountered problems

In the examples shown in precedence, we had no care to minimise the pressure drop and even the necessity of smoothing the geometry was justified by other considerations. Nevertheless, the geometry smoothing has the effect of drastically lower the pressure losses. Up to such a point that a new critical instability has been encountered during the numerical experiments. The instability has already been described and is analysed in [2]. In Figure 15, we can see that the flow in a sub-channel has stopped because of a “thermal lock”.

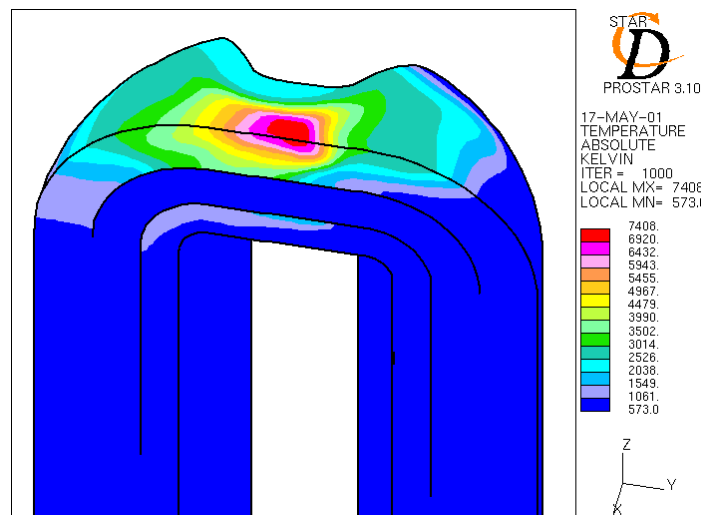


Figure 15 Illustration of a thermal lock configuration. The flow in the upper sub-channel is cannot evacuate because of the buoyancy forces, so it stops and reach unphysical temperatures. The phenomena is also present, at a lesser extend in the lowest sub-channel and nearly all the flow passes through the central one.

The insertion of localised pressure drop baffles in the numerical model allows to simply simulate pressure drop grids. In the cases shown in Figure 16, the baffles are inserted in the riser, before the

elbow and each one is given a specific pressure drop coefficient. If the coefficients are quite different with the highest in the lowest channels, then the flow is strengthened in the uppermost region, close to the free surface. In this way, the maximum temperature at the surface can be even lower than the mean outflow temperature. Obviously, this is done at the cost of heating much more the other channel and thus create strong temperature gradients which survive for long in the down-comer.

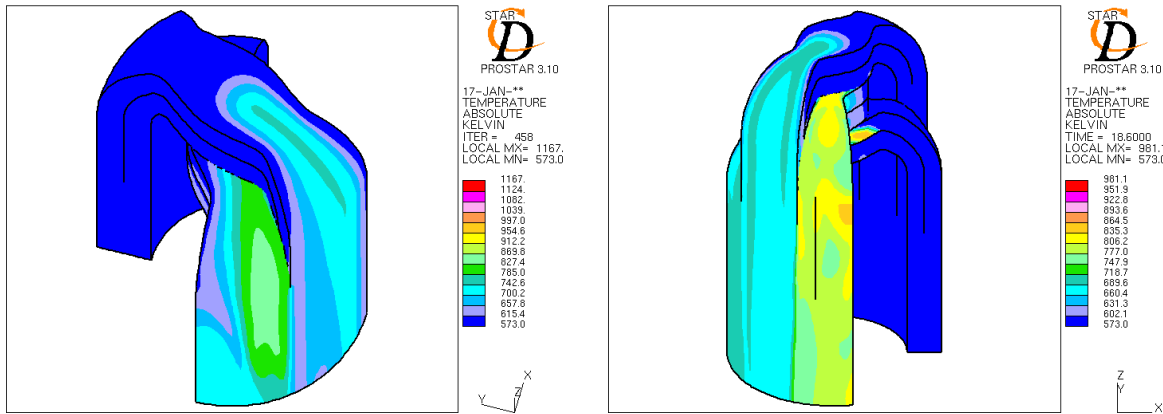


Figure 16 Two examples of multi-channel targets, with two separated channels on the left and three on the right, tested under nominal operation. The channels connect in the lower part. Each channel is separated into two sub-channels and resisting baffles have been put in inlet of each channel to control the flow splitting. The temperature field is shown. In each case, the maximum temperature is met in the interior. One can see some alteration of the symmetrical flow structure. In the right case, the surface temperature constraint is met. Unfortunately the middle channel has a much higher temperature and the outflow results unstationary.

6 Buoyancy pressure drop

While not taken into account for the pressure loss limitation, the buoyancy pressure drop is measured by the numerical simulation together with the other pressure losses. The reference pressure is taken at level 0, that is the mean free-surface level. The reference temperature and density are those of the inlet (300 C and 10327 kg/m³).

The pressure drop in the down-comer due to the buoyancy can therefore be estimated to:

$$\Delta P_b = \Delta T_{io} \times \beta \times g \times H_{down} = 115.8 \times 1.37 \times 9.81 \times 0.8 = 1250 \text{ Pa}$$

for a typical height of the computational domain of $H_{down} = 80 \text{ cm}$.

7 Beam radius optimisation

In the optimisation process, another element has to be taken into account, the beam shape. The beam energy radial distribution is basically parabolic but it can be stretched so that its foot-sprint turn from circular to ellipsoid, being therefore characterised by 2 main radius and an orientation.

For the moment, we do not know of any advantage given by an elliptic stretching. Moreover, such advantage is very likely to vanish in the multi-channel framework. Anyway, this point can be kept in mind for an optimisation limited to the single channel paradigm.

The beam shape optimisation can therefore be reduced to a beam radius (or diameter) optimisation. Most of the preceding work has been done with a diameter $D=12\text{cm}$ but some earlier simulation have been done with a diameter as small as $D=3\text{cm}$. The diameter is not likely to be made smaller than $D=3\text{cm}$ because of internal repulsion forces. On the other hand, the beam has to travel in a vacuum pipe which must be enclosed in the initial 52cm diameter cylinder.

There are advantages and drawbacks associated to small and large beam radius, the advantages of one being the drawbacks of the other. Next, we enumerate some of them:

Small beam radius advantages:

- small encumbrance and therefore more space to tailor the flow
- little buoyancy effects.

Large beam radius advantages:

- lower heat source density and therefore little sensibility to beam spatial instability
- low fluid velocity required and therefore small pressure losses
- little free-surface effects.

In () we can that the beam radius optimisation is dependent on the flow configuration and therefore on the geometry. In effect, in this particular case, a smaller beam radius gives a better result because the bigger beam radius is in some sense wider than the flow pattern.

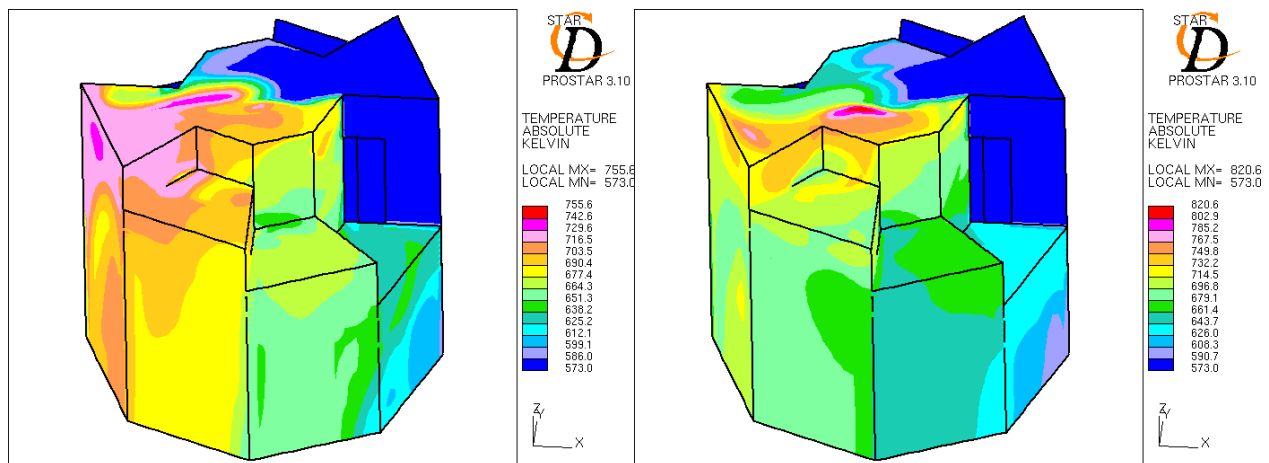


Figure 17 Temperature pattern for a geometry type described in Figure 8. The only difference between the two settings is the beam radius which is 4.5 cm on the left and 6 cm on the right. While enlarging the beam radius, the temperature maximum increases and moves from the bulk to the surface in a region of oscillating vortices.

8 Conclusions

We have given some information relative to the windowless target framework. From geometrical considerations, it seems necessary to organise finely the flow in the spallation region. The physical constraint on the pressure drop and the maximum temperature are opposed but it seems possible to

fulfil both of them. Nevertheless a critical instability may develop if one wants to minimise at most the friction losses and should be taken kept in mind during an optimisation process.

9 References

[1] Mario de Salve, personal communication Nov.2000.

[2] Windowless target instability analysis, V.Moreau Personal Note 01/03